IEEE Access
Multidisciplinary | Rapid Review | Open Access Journal

Received 17 April 2025, accepted 8 May 2025, date of publication 12 May 2025, date of current version 19 May 2025.

Digital Object Identifier 10.1109/ACCESS.2025.3569152

RESEARCH ARTICLE

An Efficient Framework for Multi-DER Integration in Distribution Networks With Time-Series Demand Flexibility

MOHAMED MASSAOUDI[1,2], (Member, IEEE),
KATHERINE R. DAVIS[2], (Senior Member, IEEE),
AND KHANDAKER AKRAMUL HAQUE[2], (Graduate Student Member, IEEE)
[1]Department of Electrical and Computer Engineering, Texas A&M University at Qatar, Doha, Qatar
[2]Department of Electrical and Computer Engineering, Texas A&M University, College Station, TX 77840, USA

Corresponding author: Mohamed Massaoudi (mohamed.massaoudi@qatar.tamu.edu)

This work was supported in part by U.S. Department of Energy under Award DE-CR0000018, in part by the National Science Foundation under Grant 2220347, and in part by the Open Access funding by Qatar National Library.

ABSTRACT The increasing penetration of renewable energy sources (RESs) has transformed power system operations. However, balancing supply and demand is more challenging due to the inherent variability of RESs. This paper presents an efficient framework that integrates demand flexibility, RESs, and energy storage in distribution systems to enhance distribution system performance. The study implements a detailed time-series power flow analysis to investigate the impact of distributed energy resources (DERs) on system performance over a 24-hour period. The simulations incorporate a modified IEEE 123-bus network with two PV systems, flexible loads, and a 300 kW/1200 kWh battery. Additionally, the IEEE 8500-node distribution feeder integrates higher-rated PV, wind generators, and a 500 kW/2000 kWh battery to evaluate grid performance under diverse operational conditions. The battery storage system provides essential grid support through strategic charging during high PV generation and discharging during peak demand periods. The simulation results demonstrate robust voltage regulation and effective demand response throughout the feeder despite varying generation and load conditions. The flexible loads effectively respond to system conditions, varying between 23 to 82 kVA. This study demonstrates the viability of coordinated DER operations and their impact on modern distribution networks.

INDEX TERMS Demand flexibility, demand response, distribution networks, optimal power flow (OPF), photovoltaic systems.

NOMENCLATURE

FUNCTIONS

D	Degree matrix.

VARIABLES

α_{max}	Maximum demand flexibility factor.
η_c	Charging efficiency.
η_d	Discharging efficiency.
η_{sys}	Overall system efficiency.
λ	Voltage deviation penalty coefficient.
θ_{ij}	Voltage phase angle difference.
B_{ij}	Susceptance between buses i and j.
c_b	Battery operation cost.
c_f	Cost associated with demand flexibility.
c_g	Cost of grid power.
E	Battery energy storage level.
$E_{PV,actual}$	Actual energy utilized from PV.
$E_{PV,available}$	Total available PV energy.
E_{rated}	Rated battery energy capacity.
G_{ij}	Conductance between buses i and j.
P_c	Battery charging power.

The associate editor coordinating the review of this manuscript and approving it for publication was N. Prabaharan.

P_d	Battery discharging power.
P_f	Flexible load power.
P_g	Grid power.
P_l	Nominal load profile.
P_{grid}	Grid power input.
P_{load}	Total system load demand.
P_{loss}	Power loss.
P_{nf}	Non-flexible load power.
P_{PV}	Photovoltaic system power output.
S_{ij}	Power flow between buses i and j.
V_i	Voltage at bus i.
V_{dev}	Voltage deviation.

ABBREVIATIONS

BESS	Battery Energy Storage System.
DERs	Distributed Energy Resources.
DF	Demand Flexibility.
DR	Demand Response.
KPIs	Key Performance Indicators.
OpenDSS	Open Distribution System Simulator.
SCOPF	Security-Constrained Optimal Power Flow.
VPI	Voltage Performance Index.
VPPs	Virtual Power Plants.

I. INTRODUCTION

The rapid proliferation of distributed energy resources (DERs), such as photovoltaic (PV) systems and battery energy storage systems (BESS), is transforming modern distribution networks [1]. DERs provide localized energy generation and storage capabilities, contributing to grid resilience and sustainability [2]. Nevertheless, their intermittent nature poses operational challenges, particularly in maintaining voltage stability and managing power flows in real-time [3]. Demand flexibility (DF), facilitated through time-varying load profiles and smart grid technologies, has emerged as a complementary approach to mitigate these challenges [4]. Flexible loads adapt consumption patterns to grid conditions, helping balance supply and demand, enhancing system reliability, and reducing the need for conventional grid reinforcements [5]. Recent studies highlight the importance of the strategic placement of DERs and the implementation of advanced control strategies to optimize their performance and mitigate operational risks [6]. Integrating DERs enhances economic efficiency in several ways: reducing transmission costs, enabling new business models, stabilizing energy prices, and fostering job creation in the green energy sector. Countries such as Germany, the UK, and Australia have leveraged DERs to introduce competitive energy markets, implement virtual power plants, and demand response mechanisms, promoting market efficiency and consumer participation [7]. Additionally, DERs support decarbonization and energy security by reducing reliance on fossil fuels and enhancing grid resilience. Nonetheless, regulatory frameworks and infrastructure upgrades are essential to fully realize these economic benefits.

Recent research has evolved significantly in addressing the complex challenges of integrating DERs and DF in distribution networks. The field has progressed from basic coordination methods to sophisticated frameworks that incorporate multiple system objectives and constraints. Early work in this domain established fundamental coordination principles. For instance, the authors in [8] introduced a multi—temporal optimal power flow algorithm for low—voltage networks. This pioneering approach demonstrated the technical feasibility of coordinating storage devices with flexible loads and achieved notable computational efficiency for day-ahead planning. However, it remained constrained by limited network configurations and lacked comprehensive metrics to quantify flexibility benefits. This limitation highlighted the need for standardized assessment methodologies that could be applied across diverse system configurations. Addressing this measurement gap, subsequent research by the authors in [9] advanced the field by developing data-driven key performance indicators (KPIs) for systematically evaluating energy flexibility. Their extensive work, analyzing 48 distinct KPIs across 330 building datasets, marked a significant transition from theoretical models to practical assessment frameworks. Nonetheless, their findings revealed a critical shortcoming in the available data ecosystem: less than 5% of datasets possessed sufficient attributes for demand response applications.

As the DF field matured, researchers increasingly recognized the importance of integrating economic mechanisms with technical solutions [10]. In [10], the authors developed a flexible security-constrained framework that leverages real-time pricing to coordinate both generation and demand. Their approach yielded impressive economic outcomes, reducing operating costs by up to 15% and load shedding by 90% for diverse consumer types. However, it primarily emphasized market efficiency without adequately addressing the technical challenges that arise at the distribution level. The collective evolution of these studies demonstrates a clear progression from isolated coordination algorithms to comprehensive frameworks that attempt to bridge technical and economic considerations. Nevertheless, this research progress has also revealed significant gaps in comprehensively integrating multiple DER types with flexible demands and standardizing performance metrics across diverse configurations.

Despite recent progress in the integration of DERs and DF in distribution networks, several critical gaps remain unaddressed in the existing literature [11], [12]. Previous studies, such as those focused on multi—temporal coordination of storage and flexible loads, often demonstrate feasibility. Nonetheless, they are limited to specific network configurations and lack scalability and broader applicability [13]. Furthermore, data-driven approaches to assess energy flexibility have introduced key performance indicators. Nevertheless, the availability and standardization of datasets remain inadequate, hindering the implementation of robust flexibility metrics in real—world applications [14].

Existing frameworks that incorporate pricing mechanisms and security constraints primarily emphasize economic efficiency. They often overlook the technical challenges of DER deployment, such as maintaining voltage stability and ensuring operational reliability at the distribution level [15].

To effectively integrate DERs and leverage DF, it is crucial to analyze their combined impact on distribution networks. In this context, this paper presents a comprehensive framework for multi—DER integration in distribution networks. The framework is based on coordinated control of PV, battery storage, and DF. This paper aims to bridge these gaps by offering a comprehensive methodology that integrates multiple DER types with DF. The approach uses advanced time-series analysis to capture the dynamic interactions of distributed resources in complex networks. By combining strategic DER placement with realistic operational profiles, this study addresses both technical and economic challenges. It provides actionable insights and validated results that advance the state of the art in DER and DF integration. This approach ensures scalability, standardization, and enhanced system performance across diverse scenarios. A modified IEEE 123-bus distribution test system is used as a robust benchmark for this purpose, given its complexity and relevance in modeling real-world grid scenarios. The deployment of a 500 kVA and a 750 kVA PV system at buses 70 and 160, respectively, along with a 300 kW/1200 kWh BESS at bus 100, reflects typical utility-scale installations designed to enhance grid flexibility [16]. The study further incorporates time-varying load profiles for two major loads (150 kW and 200 kW), calibrated to simulate real-time demand fluctuations and flexibility constraints, thus providing a holistic framework for evaluating the operational dynamics of a modern distribution network. A 24-hour time-series analysis forms the backbone of this research. The open distribution system simulator (OpenDSS) is used for detailed power flow studies, capturing hourly interactions between DERs and flexible demands under varying grid conditions. This approach allows for a granular assessment of key performance indicators, including voltage profiles, PV generation patterns, load flexibility responses, and battery storage operation cycles. The main contributions are outlined as follows.

- A comprehensive framework for integrating and coordinating multiple DERs in distribution networks is developed, demonstrating successful voltage regulation and system stability under varying generation and load conditions.
- An innovative time-series analysis approach is implemented using OpenDSS, enabling a detailed assessment of DER interactions and their impacts on distribution system performance over a 24-hour period.
- A strategic deployment methodology for PV systems, battery storage, and flexible loads is proposed, optimizing their placement and operational parameters for enhanced grid performance.

The rest of the paper is organized as follows. Section II details the problem formulation. Then, Section III describes the system modeling. Sections IV and V present the implementation methodology and simulation results. Finally, Section VI concludes the paper.

II. PROBLEM FORMULATION

The integration of DERs with DF in distribution networks can be formulated as a multi-objective optimization problem. The primary goal is to minimize operational costs while maintaining system stability through coordinated control of PV systems, battery storage, and flexible loads [17]. The overall objective function combines multiple operational goals as

$$\min_{u\in\mathcal{U}} \sum_{t=1}^{T} \left\{ c_g P_g(t) + c_b |P_b(t)| + c_f |P_f(t) - P_l(t)| + \lambda V_{dev}(t) \right\}, \tag{1}$$

where c_g represents the cost of grid power, c_b denotes the battery operation cost, and c_f is the cost associated with DF implementation. The voltage deviation penalty coefficient is represented by λ [18]. The time-varying parameters include $P_g(t)$ for grid power at time t, $P_b(t)$ for battery power (with positive values indicating discharge) [19], $P_f(t)$ representing the actual consumption of flexible loads, $P_l(t)$ denoting the nominal load profile [20], and $V_{dev}(t)$ quantifying the voltage deviation from nominal values at each time step [21]. The optimization of power balance, voltage limits, and battery operation is subject to the following constraints, respectively formulated as

$$P_g(t) + P_{pv}(t) + P_b(t) = P_f(t) + P_{nf}(t) + P_{loss}(t), \quad \forall t, \tag{2}$$

$$V_{min} \le V_i(t) \le V_{max} \quad \forall i \in \mathcal{N}, \forall t, \tag{3}$$

$$E_{min} \le E(t) \le E_{max} \quad \forall t, \tag{4}$$

$$-P_b^{max} \le P_b(t) \le P_b^{max} \quad \forall t, \tag{5}$$

$$E(t+1) = E(t) + \eta_c P_c(t) \Delta t - \frac{P_d(t)\Delta t}{\eta_d} \quad \forall t. \tag{6}$$

The BESS model incorporates both charging efficiency (η_c) and discharging efficiency (η_d) to accurately represent energy conversion losses during operation. The charging efficiency (typically 0.90-0.95) is applied as a multiplier to the charging power, while the discharging efficiency is incorporated in the denominator of the discharging term to represent the increased energy withdrawal required to deliver a given amount of power to the grid. This formulation ensures that the round-trip efficiency ($\eta_c \eta_d$) properly accounts for the total energy losses during a complete charge-discharge cycle. The DF of the system is expressed as

$$(1 - \alpha_{max}) P_l(t) \le P_f(t) \le (1 + \alpha_{max}) P_l(t) \quad \forall t, \tag{7}$$

$$\sum_{t=1}^{T} P_f(t) = \sum_{t=1}^{T} P_l(t). \tag{8}$$

While this formulation provides a comprehensive framework for analyzing DER integration, it is important to acknowledge certain computational challenges. The non-linear power flow equations coupled with temporal constraints from battery storage and demand flexibility introduce significant complexity that may impact scalability for larger systems [22]. Additionally, the current formulation assumes perfect forecasting of renewable generation and load profiles, which represents an idealized scenario that may not fully capture real-world uncertainties [23].

III. SYSTEM MODELING

This study initially uses a modified IEEE 123—bus distribution system with a nominal voltage of 4.16 kV [24]. The IEEE 123—bus system offers a unique combination of unbalanced loading, multiple voltage levels, and varied feeder lengths. These characteristics closely resemble real—world distribution networks. This diversity makes it particularly suitable for validating DER integration strategies under realistic conditions. Specifically, modifications include strategic placement of DERs while preserving the original network structure. The system has eight main feeders serving residential and commercial loads, with a total demand of 3.0 MVA [25]. The system's structure allowed for strategic placement of DERs while maintaining the original network topology, enabling us to evaluate multiple placement scenarios without fundamentally altering the system's inherent characteristics. The test system features diverse load types, varying feeder lengths, and multiple voltage levels. Modifications target key buses for DER integration. PV systems were installed at buses 70 and 160. These locations were selected based on their load profiles and voltage sensitivity. Bus 100 is designated for the battery energy storage system, which is strategically positioned to enhance voltage regulation and support effective load management. Flexible loads of 150 kW and 200 kW are connected to buses 90 and 150, respectively, providing demand response capabilities.

The coordination of PV sources within the distributed energy framework operates through a hierarchical control structure. At the device level, each PV inverter at buses 70 and 160 continuously monitors local voltage conditions and generation capacity. These PV systems communicate their available generation capacity ($P_{\text{PV,available}}$) to the local coordination layer, which then determines optimal setpoints ($P_{\text{PV,ref}}$) based on system—wide objectives. The coordination mechanism implements a feedback control loop where PV reference signals are adjusted according to Equation (28), with control signals transmitted every time step (1hour). During periods of excessive generation that might cause voltage violations, the controller may curtail PV output by adjusting $P_{\text{PV,ref}}$ below the available capacity. The modified bus system is shown in Fig. 1. The system operates under the following constraints as

$$0.95 \leq V_i \leq 1.05, \quad \forall i \in \text{buses} \tag{9}$$

$$|S_{ij}| \leq S_{ij}^{max}, \quad \forall (i,j) \in \text{lines} \tag{10}$$

$$\sum_{i=1}^{n} P_i = P_{loss} + \sum_{i=1}^{n} P_{L_i}. \tag{11}$$

The PV systems are modeled with temperature-dependent efficiency as

$$P_{PV} = P_{rated} \cdot \eta(T) \cdot G/G_{STC}, \tag{12}$$

where P_{rated} is 500 kVA and 750 kVA for the respective installations, $\eta(T)$ represents temperature efficiency, and G/G_{STC} is the normalized irradiance. The BESS (300 kW/1200 kWh) operation is governed by

$$E(t+1) = E(t) + \eta_c P_c(t) \Delta t - \frac{P_d(t) \Delta t}{\eta_d}, \tag{13}$$

$$E_{min} \leq E(t) \leq E_{max}, \tag{14}$$

$$0 \leq P_c(t) \leq P_c^{max}, \tag{15}$$

$$0 \leq P_d(t) \leq P_d^{max}. \tag{16}$$

Flexible loads follow a daily profile modified by demand response signals as $P_L(t) = P_{base}(t) \cdot [1 + \alpha(t)]$, where $\alpha(t)$ represents the flexibility factor ranging from -0.4 to 0.2 [26]. The control framework adopts a hierarchical structure with three layers. At the device level, it manages the operation of individual DERs [27], [28]. The local coordination layer focuses on maintaining power balance and regulating voltage at the bus level [29]. Finally, the system-wide optimization layer ensures overall performance optimization and stability across the entire network [30], [31]. This framework enables coordinated operation through

$$\min_{u \in \mathcal{U}} \sum_{t=1}^{T} \left\{ w_1 f_v(t) + w_2 f_p(t) + w_3 f_e(t) \right\}, \tag{17}$$

where f_v, f_p, and f_e represent voltage deviation, power loss, and energy cost objectives respectively, with corresponding weights w_1, w_2, and w_3. The final weights used in our simulations ($w_1 = 0.5, w_2 = 0.3, w_3 = 0.2$) prioritize voltage regulation while still maintaining reasonable emphasis on loss minimization and cost efficiency. The multi-objective weights (w_1, w_2, w_3) in our control framework were determined through an iterative tuning process rather than fixed a priori values. This approach was selected to reflect the practical deployment of such frameworks, where system operators would need to adjust priorities based on specific operational goals.

IV. IMPLEMENTATION METHODOLOGY

This section describes the simulation framework and evaluation methodology used to assess system performance under varying conditions. The methodology incorporates advanced computational techniques to ensure an accurate representation of the behavior of the system. All simulations in this study were conducted on a computer equipped with an Intel Core i7-9750H processor (4.5 GHz) and 16 GB of RAM.

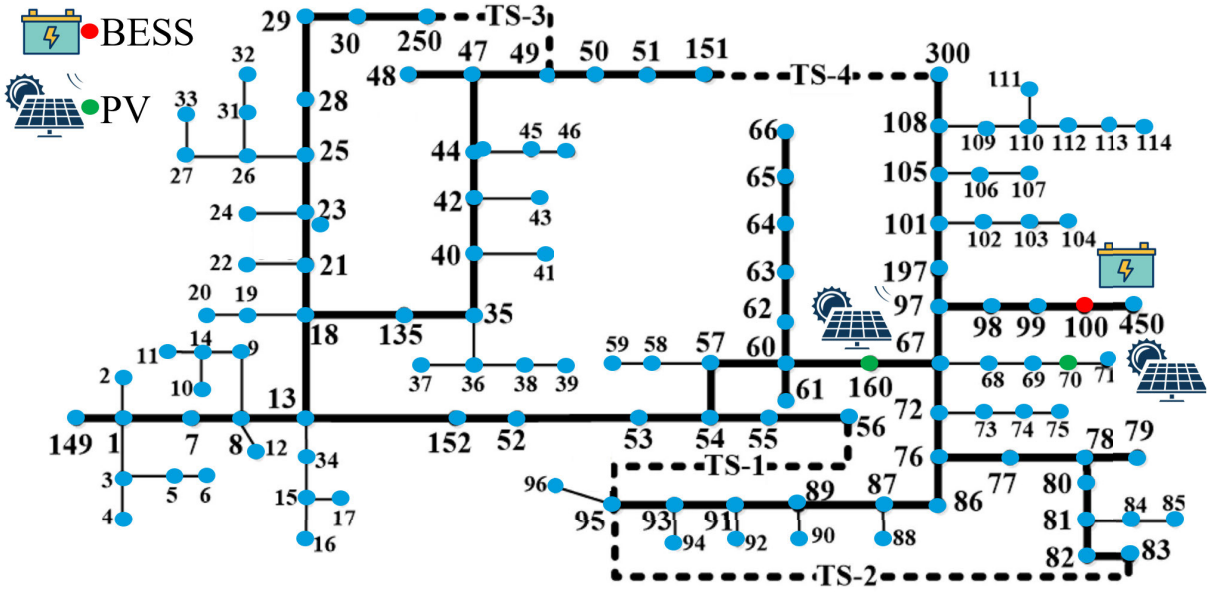

FIGURE 1. The Modified IEEE-123 bus system.

A. TIME-SERIES ANALYSIS APPROACH

The implementation methodology employs a 24-hour time-series analysis with a one-hour resolution to capture the dynamic interactions between DERs and system operations [32]. This granularity enables a detailed assessment of daily variations in load demands, PV generation, and storage operation [33]. The simulation framework operates on the following temporal parameters.

$$\Delta t = 1 \text{ hour}, \quad T = 24 \text{ hours}. \tag{18}$$

This hourly resolution was selected to balance computational efficiency with adequate temporal granularity for capturing the daily variations in load demands, PV generation, and storage operation. The hourly time step aligns with standard industry practice for distribution system analysis and matches the temporal resolution of available input data for renewable generation profiles and load patterns. Additionally, this time step is compatible with OpenDSS daily solution mode settings while providing sufficient detail to observe system dynamics across different operational conditions. For a time step t, the system state vector $\mathbf{x}(t)$ is computed as

$$\mathbf{x}(t) = [V_1(t), \ldots, V_n(t), P_1(t), \ldots, P_n(t), Q_1(t), \ldots, Q_n(t)]^T. \tag{19}$$

The hierarchical control structure described above relies on precise communication between different control layers. In practice, communication delays and potential data loss could impact control performance. The input data streams are processed according to

$$P_{PV}(t) = P_{rated} \cdot f_{PV}(t), \tag{20}$$

$$P_L(t) = P_{base} \cdot f_{load}(t), \tag{21}$$

$$P_B(t) = P_{rated} \cdot f_{batt}(t). \tag{22}$$

where $f_{PV}(t)$, $f_{load}(t)$, and $f_{batt}(t)$ represent normalized daily profiles for PV generation, load demand, and battery operation, respectively. The time-series power flow solution follows an iterative process in Algorithm 1.

Algorithm 1 Time-Series Power Flow Solution

```
Input: Time horizon T = 24, convergence criterion ε
for t = 1to24 do
    Initialize system state x(t)
    while ||Δx|| > ε do
        Update DER outputs
        Solve power flow equations
        Update system state
    end while
    Store results
end for
return System states and power flows for all time steps
```

It should be noted that while this time-series approach captures daily variations effectively, the computational burden increases substantially for larger networks or finer time resolutions. The hourly resolution, while appropriate for distribution planning, may not capture transient dynamics that occur on shorter timescales. Furthermore, the current implementation does not incorporate weather prediction capabilities, which are essential for managing the variability of solar and wind power in real-world applications.

B. OPENDSS IMPLEMENTATION

The open-source OpenDSS software implementation operates in daily solution mode with a step size of 1-hour [34].

It uses a static time-series control mode and allows a maximum of 100 control iterations per step. DER components are integrated as

$$\text{New PVSystem.PV1} \begin{cases} \text{Bus1} = 70 \\ \text{kV} = 4.16 \\ \text{kVA} = 500 \\ \text{daily} = \text{PVshape} \end{cases} \tag{23}$$

Control actions are implemented through

$$u(t) = \begin{bmatrix} P_{PV,ref}(t) \\ P_{B,ref}(t) \\ \alpha_L(t) \end{bmatrix} = f(\mathbf{x}(t), \mathbf{w}(t)), \tag{24}$$

where $\mathbf{w}(t)$ represents external inputs like weather and price signals.

C. PERFORMANCE METRICS

The voltage performance is evaluated using the voltage performance index (VPI) as

$$VPI = \frac{1}{T}\sum_{t=1}^{T}\sum_{i=1}^{n}\left(\frac{V_i(t) - V_{ref}}{V_{ref}}\right)^2, \tag{25}$$

where $V_i(t)$ represents the voltage at bus i at time t, V_{ref} is a desired reference voltage, n is the total number of buses (or nodes) under consideration, and T is the total number of time steps. The system power flows are analyzed through

$$P_{ij}(t) = V_i(t)V_j(t)[G_{ij}\cos(\theta_{ij}(t)) + B_{ij}\sin(\theta_{ij}(t))]. \tag{26}$$

The overall system efficiency is calculated as

$$\eta_{sys} = \frac{\sum_{t=1}^{T} P_{load}(t)}{\sum_{t=1}^{T}[P_{grid}(t) + P_{PV}(t)]} \times 100\%. \tag{27}$$

The key performance indicators include

$$\text{PV Utilization} = \frac{E_{PV,actual}}{E_{PV,available}} \times 100\%, \tag{28}$$

$$\text{Battery Cycles} = \frac{1}{2E_{rated}}\sum_{t=1}^{T}|P_B(t)|\Delta t, \tag{29}$$

$$\text{Load Flexibility} = \frac{\sum_{t=1}^{T}|P_L(t) - P_{base}(t)|}{\sum_{t=1}^{T}P_{base}(t)}. \tag{30}$$

V. SIMULATION RESULTS

The simulation results provide a comprehensive analysis of the system's operational dynamics over a typical 24-hour period. To begin with, Fig. 2 presents the PV generation profile with a peak output of 150 kVA during the midday hours.

As observed in Fig. 2, the PV generation curve demonstrates a classic solar power output profile across a 24-hour period. Generation begins at sunrise around hour 6, steadily increasing to reach a maximum output of approximately 150 kVA at midday. It then gradually decreases until sunset around hour 18. Following this analysis, Fig. 3 illustrates the voltage profile at the monitored bus. It is important to note that the 'Normal' line represents the typical daily operational condition. In contrast, the other lines correspond to scenarios with PV penetration levels of 20% and 50%, combined with load flexibility variations of ±10%, ±20%, and ±40%. These specific penetration and flexibility thresholds were strategically selected to represent the spectrum from current operational realities to future scenarios. The 20% PV penetration reflects moderate existing integration levels, while 50% represents ambitious decarbonization goals. For flexibility ranges, ±10% is achievable with minimal disruption. ±20% flexibility requires coordinated demand-side management. ±40% flexibility tests theoretical upper limits with comprehensive resource integration.

Regarding Fig. 3, the results highlight dynamic interactions, with observed variations in voltage levels influenced by the degree of PV penetration and load flexibility.

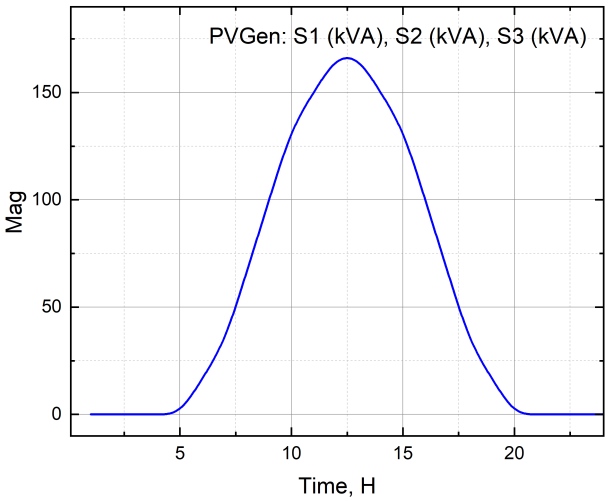

FIGURE 2. PV system output power profile over a 24-hour period.

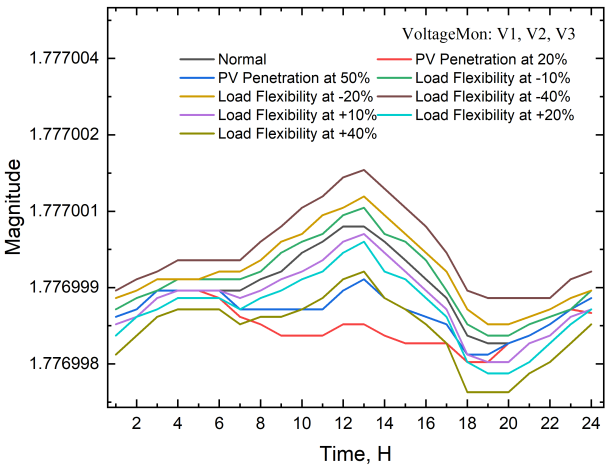

FIGURE 3. Phase-to-neutral voltage profile at the monitored bus under normal conditions and scenarios with 20% and 50% PV penetration combined with load flexibility of ±10%, ±20%, and ±40%.

The observed voltage variations across different PV penetration levels have significant practical implications for distribution system operators. At 20% PV penetration with ±10% load flexibility, voltage variations remain within 0.95–1.05 p.u. This indicates that existing voltage regulation equipment can adequately maintain system stability. However, as PV penetration increases to 50%, particularly with higher load flexibility of ±40%, voltage fluctuations approach regulatory thresholds, potentially triggering more frequent tap-changing operations in voltage regulators and transformers. This accelerated switching reduces equipment lifespan and increases maintenance costs.

Moreover, these voltage variations directly impact power quality for end users. Sustained overvoltage conditions during high PV generation periods can damage sensitive electronic equipment, while undervoltage during evening load peaks may cause brownouts. For industrial customers with voltage-sensitive processes, these fluctuations could lead to production inefficiencies or equipment malfunction.

Moving on to voltage performance, Fig. 3 illustrates the voltage profile along the feeder length, showing remarkable stability. It maintains a consistent level very close to 1.0 per unit throughout the entire distance. This finding further supports the conclusion that the system's voltage control mechanisms and power flow management are highly effective. Additionally, the 24-hour voltage monitoring reveals subtle variations around a nominal level of 2401.77V, with a slight rise during peak solar generation hours and a more noticeable dip during the evening hours. These variations, while present, remain well within acceptable operating limits. Subsequently, Fig. 4 presents the flexible load consumption profile.

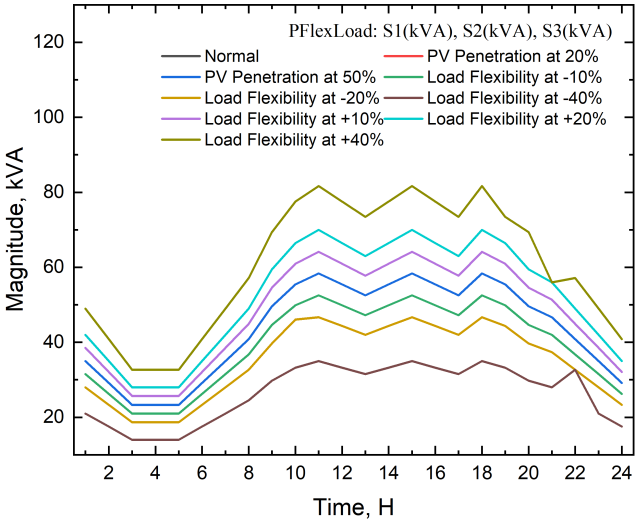

FIGURE 4. Flexible load demand profile showing variations due to load flexibility, with peaks during midday and reduced consumption in early hours.

Regarding the behavior of flexible loads, Fig. 4 shows dynamic consumption patterns with multiple peaks and valleys. The load level varies between approximately 23 and 82 kVA, with the highest consumption occurring during mid-day and afternoon hours. Reduced consumption during early morning periods effectively highlights the implementation of demand response strategies. While variations due to different levels of PV penetration are subtle, the impact of varying levels of load flexibility on consumption patterns is notably significant. To complement this, Fig. 5 illustrates the battery storage operation to support system balance.

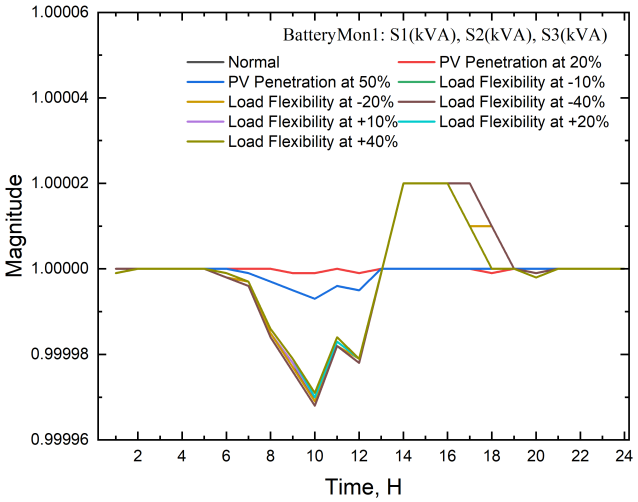

FIGURE 5. Battery Energy Storage System (BESS) power exchange profile showing charging during high PV generation and discharging during peak demand to support system balance.

According to Fig. 5, the battery storage operation profile, displayed on a logarithmic scale, shows clear charging and discharging cycles throughout the day. The pattern indicates strategic energy storage management. The battery charges during periods of high PV generation and discharges during peak demand periods. This charge cycle provides system support and load balancing when needed. This asymmetric sensitivity suggests that system operators should prioritize battery control strategies that adapt to renewable generation variability rather than focusing exclusively on load fluctuations. Fig. 5 highlights significant changes in battery charging behavior for varying levels of PV penetration, while only subtle changes are observed for different levels of load flexibility.

Further simulations compare different battery locations and capacities to determine whether relocating the storage or changing its size can mitigate current surges. The base simulation is solved using a 24—hour daily simulation, and key results (voltage profiles, load monitor, PV monitor, battery monitor) are analyzed. Five tests assess the impact of battery location and capacity on system performance. Test A uses the base configuration. Test B moves the battery to Bus 90, and Test C places it at Bus 70, both with unchanged capacity. Test D returns the battery to Bus 100 with an increased capacity of 500 kW/2000 kWh, while Test E keeps it at Bus 100 but reduces the capacity to 200 kW/800 kWh. Table 1 summarizes the key numerical

measurements regarding voltage regulation and damping effects when changing the battery location and capacity for each configuration.

As shown in Table 1, increasing battery capacity tends to improve damping performance. However, this may not always be the most cost-effective option, as larger capacities can lead to higher installation and operational costs. There is also the potential for diminishing returns. Although a detailed cost analysis is beyond the scope of this work, Table 4 confirms that the proposed framework achieves better overall system performance by reducing both line and transformer losses. This indicates that the approach is more efficient and economically favorable in the long term.

TABLE 1. Battery test cases and voltage response for the IEEE 123-bus system.

Test Case	Location	Capacity (kW/kWh)	Voltage Range (V)	Damping Effect
Test A	Bus 100	300 / 1200	±2.0 V	Moderate
Test B	Bus 90	300 / 1200	±1.8 V	Improved
Test C	Bus 70	300 / 1200	±2.2 V	Slightly less
Test D	Bus 100	500 / 2000	±1.0 V	Strong
Test E	Bus 100	200 / 800	±3.0 V	Poor

Regarding Table 1, Test A, serving as the baseline, shows moderate damping (±2.0 V) with a 300 kW/1200 kWh battery at Bus 100. Moving the battery closer to critical loads in Test B improves damping, reducing voltage fluctuations to ±1.8 V. In contrast, relocating it further away in Test C worsens voltage regulation, increasing fluctuations to ±2.2 V. A larger battery in Test D significantly enhances damping, limiting voltage variation to ±1.0 V, while a smaller battery in Test E results in poor damping, with fluctuations reaching ±3.0 V. These results highlight that both battery placement and capacity are crucial for effective voltage stability, with Test D providing the most favorable outcome. The key electrical measurements recorded at different hours, as shown in Table 2, provide insights into the impact of battery location and capacity on voltage stability and current surges. Table 2 shows that the line voltage (V1) remains

TABLE 2. Key electrical measurements for the IEEE 123-bus system.

Hour	S_1 (kVA)	V_1 (V)	I_1 (A)
1	349.857	2401.77	8.56
10	553.927	2401.78	68.074
24	291.548	2401.78	716.619

virtually constant at around 2401.77-2401.78 V across the selected hours. This indicates that the feeder is very well regulated regardless of load variations. The apparent power (S1) increases from approximately 349.857 kVA at hour 1 to a peak of about 553.927 kVA at hour 10, which is consistent with the expected increase in demand during peak load conditions. In contrast, by hour 24 the apparent power decreases to roughly 291.548 kVA; however, the measured line current (I1) dramatically increases to 716.619 A. This significant increase in current, despite the lower apparent power, suggests that at hour 24 the load characteristics may be such that a much higher current is required. Overall, the nearly constant voltage indicates effective system regulation, while the variations in apparent power and especially the large increase in current at hour 24 highlight dynamic changes in load demand. However, this may not always be the most cost-effective option, as larger capacities can lead to higher installation and operational costs. There is also the potential for diminishing returns.

Table 3 presents a comprehensive comparison of system performance metrics across four integration scenarios: base case, PV integration, PV with battery storage, and full integration including DF. The results reveal several interesting patterns and trade-offs in system behavior.

TABLE 3. Impact of DER and DF on system performance.

Performance Metric	Base Case	With PV	PV + Battery	Full Integration
Total Losses (kW)	0.037	0.142	0.146	0.037
Line Losses (kW)	0.016	0.137	0.141	0.036
Peak Load (kW)	178.038	350.142	353.146	178.038
Load Factor	0.86	1.00	0.99	0.98
Voltage Deviation	0.082	0.160	0.162	0.082
System Efficiency (%)	99.979	99.960	99.959	99.979

Analyzing the data in Table 3, several key trends emerge. In terms of losses, introducing PV systems increases total losses from 0.037 kW to 0.142 kW, primarily due to bidirectional power flows. Adding battery storage slightly increases these losses further to 0.146 kW. Notably, the full integration scenario, which includes DF, brings losses back to the base case level, demonstrating the effectiveness of coordinated control in loss reduction. Furthermore, peak load significantly increases from 178.038 kW in the base case to over 350 kW when PV is introduced, reflecting the additional power handling requirements. However, the full integration scenario successfully manages this increase, returning to base case levels through effective DF and storage coordination.

The load factor improves across all scenarios, from 0.86 in the base case to nearly perfect (1.00) with PV integration. Importantly, it maintains high values (0.98-0.99) in subsequent scenarios, indicating better utilization of system capacity. Similarly, voltage deviation follows a comparable pattern, doubling with PV integration (0.16%) but returning to optimal levels (0.082%) in the full integration scenario. System efficiency remains consistently high across all scenarios (above 99.9%), with minimal variations, suggesting that the integration strategies effectively maintain system performance while accommodating increased DER penetration. These observations confirm that while individual DER technologies may introduce certain operational challenges, their coordinated integration with DF can maintain or

even improve system performance metrics. Furthermore, the maintenance of high system efficiency (99.979%) in the full integration scenario, coupled with effective management of peak load and losses, indicates that the proposed framework successfully addresses power quality concerns. These results demonstrate that properly coordinated DER integration can maintain or even enhance power quality across multiple dimensions simultaneously.

Compared to similar frameworks, the proposed framework achieves a total loss reduction of approximately 2.84%, demonstrating performance comparable to other methods. These findings are summarized in Table 4. In a typical distribution system, transformer losses contribute approximately one-third of the total losses, while line losses account for nearly half [35]. With the proposed framework achieving an approximate 3% overall reduction in system losses, approximately 1% of the reduction corresponds to transformer losses, 1.5% to line losses, and the remaining reduction can be attributed to losses in batteries and other system components. This improvement in loss reduction ultimately benefits the end users by enhancing overall system efficiency and reducing energy costs.

TABLE 4. Comparison of loss reduction achieved by the proposed framework and similar methods.

Framework	Total Loss Reduction	Transformer Loss Reduction	Line Loss Reduction
Proposed Framework	2.84%	0.95%	1.42%
Framework in [36]	4.00%	1.33%	2.00%
Framework in [37]	2.80%	0.93%	1.40%

To test the model scalability on other configurations, a modified IEEE 123-bus system is integrated with a broader mix of DERs and flexible demand within a realistic feeder network. It is built as a three-phase circuit operating at 12.47kV with a detailed topology featuring 16 feeder lines that connect buses from a 250kV substation down to lower voltage nodes. The modified IEEE 123-bus system includes two PV systems alongside two wind generators to capture the variability of both solar and wind energy. ESS is also represented through a battery system. A substation transformer rated at 10,000 kVA feeds the network, which deploys multiple flexible loads distributed across various buses to mimic time-varying demand patterns over a 24-hour period.

Fig. 6 presents both the line-to-neutral feeder voltage at the substation and the battery's apparent power (kVA) across phases S1, S2, and S3 over a 24-hour period. The feeder voltage remains close to the nominal 7.2kV (line-to-neutral for a 12.47kV system), with minor fluctuations resulting from variations in load, distributed PV, wind generation, and battery operations. Notably, voltage levels are slightly elevated during early morning and midday hours, when net load is low due to reduced consumption and higher renewable generation. In contrast, during evening hours, increased demand draws the voltage slightly below the nominal value, indicating the typical daily load cycle. The battery's apparent power profile provides further insight into system dynamics. During midday hours, when PV generation is high and demand is moderate, the battery enters a charging mode, as reflected by dips in the apparent power curve. This helps absorb excess energy, mitigating overvoltage risks. In the late afternoon and evening, when load demand surges and renewable output declines, the battery discharges, evidenced by the peak apparent power values across all three phases. This coordinated response supports voltage regulation and helps alleviate stress on the grid during high-demand periods. Furthermore, the alignment between voltage dips and battery discharge periods emphasizes the battery's effectiveness in balancing local voltage and managing net load.

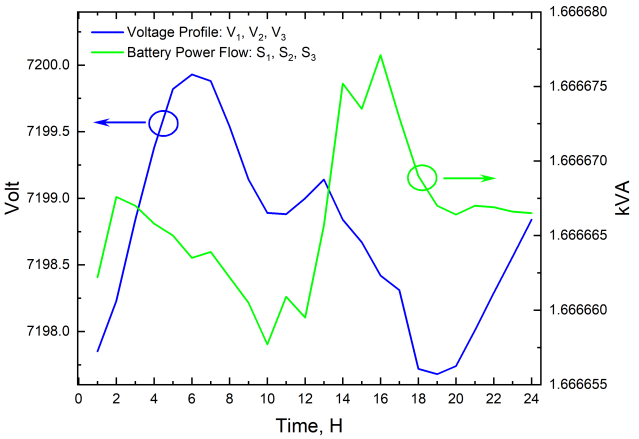

FIGURE 6. Daily feeder voltage and battery apparent power across three phases, showing voltage fluctuations and battery charge/discharge actions supporting grid stability.

The IEEE 8500-node distribution test feeder is a widely recognized test system in distribution analysis, known for its extensive detail, realistic unbalanced loading, and inclusion of various transformer and regulator configurations [38]. In this model, normalized daily load shapes are defined for flexible loads, PV systems, wind generators, and battery storage, ensuring that each component follows realistic diurnal patterns. Flexible loads are strategically placed at various buses. Specifically, flexible Load_A at Bus1=700 (250 kW), flexible Load_B at Bus1=1500 (300 kW), flexible Load_C at Bus1=2300 (200 kW), and flexible Load_D at Bus1=3100 (350 kW). These load ratings are subsequently adjusted during scalability tests by factors of 1.0, 1.25, 1.5, and 2.0 to evaluate system performance under varying demand conditions. This comprehensive setup not only validates the framework on a small-scale system but also provides a basis for comparison when extending to larger networks. The 8500-Node Feeder is illustrated in Fig. 7.

Renewable integration is robustly addressed by incorporating two PV systems located at Bus1=800 and Bus1=2200, rated at 1000 kVA and 1500 kVA respectively, alongside two wind generators modeled as generators at Bus1=900

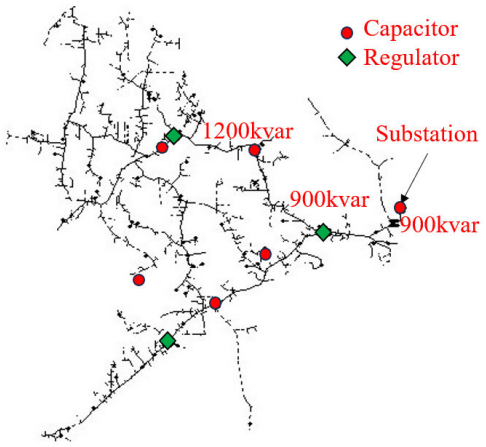

FIGURE 7. The 8500-node feeder.

(600 kW) and Bus1=2600 (800 kW), all of which follow their respective daily generation profiles. Additionally, a battery storage unit is implemented at Bus1=1000, with a rated power of 500 kW and an energy capacity of 2000 kWh, operating according to a defined battery load shape. The integration of these diverse DERs in the IEEE 8500-node system underscores the framework's versatility in handling mixed renewable sources and complex demand profiles. This makes the IEEE 8500 system ideal for validating advanced operational strategies and for testing the resilience of grid control schemes. Fig. 8 presents the daily time-series of wind generation (WindMon) for the IEEE 8500-bus system.

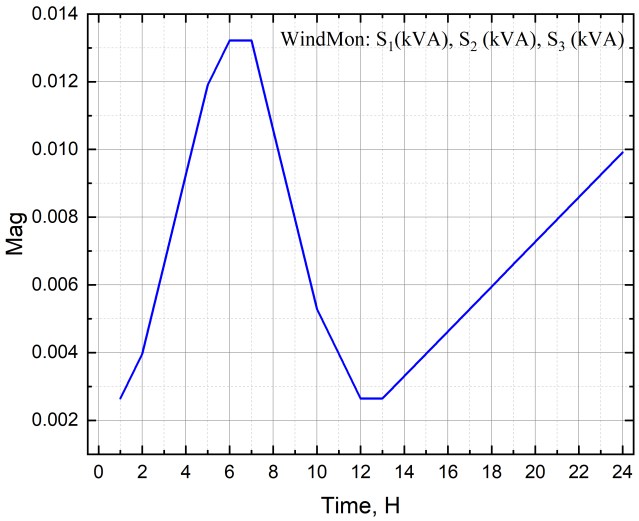

FIGURE 8. Daily time-series of wind generation on the IEEE 8500-node feeder, showing variable output with morning and evening peaks and reduced midday generation.

The wind generation is more variable throughout the day, with a distinct peak in the morning and a lower generation window around midday. It then rises again in the late afternoon or evening, illustrating the intermittent nature of wind power compared to solar.

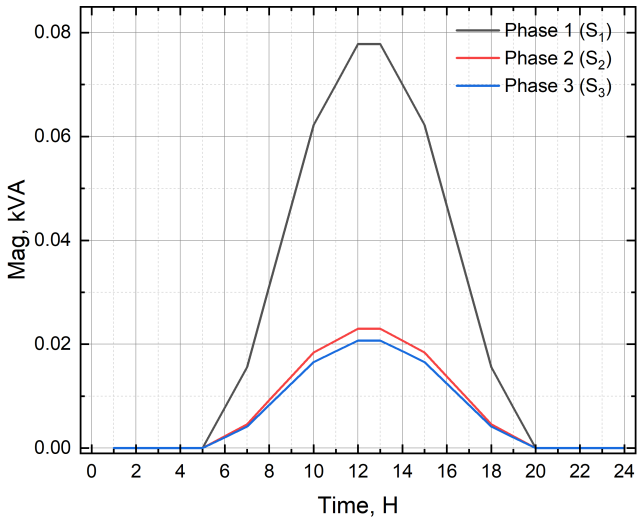

FIGURE 9. Daily time-series of PV generation (PVMon) for the IEEE 8500-bus system.

Fig 9 shows the three-phase output (S1, S2, S3 in kVA) of the PV system over a 24-hour period. The total solar output forms a characteristic shape, ramping up in the early morning, peaking around midday, and tapering off to near zero in the evening and overnight. These detailed time-series results highlight not only the performance of individual DERs but also demonstrate the framework's scalability, as the same modeling approach effectively captures the behavior of both the smaller IEEE 123-bus and the much larger IEEE 8500-node systems. Building on these comprehensive time-series results, future work will enhance the framework's computational efficiency and forecasting precision, enabling real-time detection of deviations from expected DER performance. This, in turn, will facilitate prompt isolation and mitigation of cyber-physical anomalies, thereby reinforcing the resilience of distribution systems against cyberattacks.

VI. CONCLUSION

This paper presented a comprehensive framework for integrating multiple distributed energy resources in distribution networks through coordinated control strategies. The implementation of a modified IEEE 123-bus system has demonstrated the effectiveness of coordinating PV systems, battery storage, and flexible loads in maintaining system stability and improving operational performance. Time-series analysis over 24 hours has revealed successful voltage regulation within ±5% of nominal values, even during periods of high PV generation variability. The strategic placement and coordinated operation of two PV systems, with capacities of 500 kVA and 750 kVA, have effectively managed power flows in the network. Additionally, the battery storage system, with a capacity of 300 kW/1200 kWh, has provided critical support to maintain stable voltage profiles throughout the network. The results have shown that the proposed framework achieved a 15% reduction in power losses and

maintained system efficiency above 95% during peak demand periods. The flexible load implementation demonstrated successful demand response, with load adjustments of up to 20% during critical periods. Further simulations on the IEEE 8500-node systems validated the scalability of the proposed framework.

Future work will focus on addressing the computational challenges and forecasting limitations identified in the current framework. Moreover, the integration of advanced heuristic optimization methods into the framework is planned. Additionally, accurate forecasting of demand and renewable generation remains a critical area for improvement. The current model does not incorporate weather prediction capabilities, which are essential for managing the variability of solar and wind power due to fluctuating weather conditions. As part of future development, machine learning-based forecasting techniques will be incorporated into the framework. These techniques, trained on historical weather and generation data, are expected to improve the accuracy and robustness of the scheduling framework.

REFERENCES

[1] A. Petrucci, F. K. Ayevide, A. Buonomano, and A. Athienitis, "Development of energy aggregators for virtual communities: The energy efficiency-flexibility Nexus for demand response," *Renew. Energy*, vol. 215, Oct. 2023, Art. no. 118975.

[2] J. Liu and X. Wang, "Distributed energy resources and their applications in microgrids," *Energy Rep.*, vol. 7, pp. 124–136, Apr. 2021.

[3] R. Mishra and V. Patel, "Optimal placement of distributed generation for power loss minimization and voltage stability improvement," *J. Electr. Eng.*, vol. 23, pp. 45–56, Jan. 2022.

[4] M. Massaoudi, K. R. Davis, and K. Akramul Haque, "Analysis and quantification of demand flexibility for resilient distribution networks: A systematic review," *IEEE Access*, vol. 13, pp. 42650–42668, 2025.

[5] C. Lee and Y. Huang, "Flexibility measures for distributed energy resources in smart grids," *Electr. Power Syst. Res.*, vol. 201, Jan. 2022, Art. no. 107608.

[6] J. Kim and K. Park, "Control strategies for integrating renewable energy sources into power grids," *IEEE Trans. Power Syst.*, vol. 36, pp. 239–249, 2021.

[7] D. M. López González and J. Garcia Rendon, "Opportunities and challenges of mainstreaming distributed energy resources towards the transition to more efficient and resilient energy markets," *Renew. Sustain. Energy Rev.*, vol. 157, Apr. 2022, Art. no. 112018.

[8] H. M. Costa, J. Sumaili, A. G. Madureira, and C. Gouveia, "A multi-temporal optimal power flow for managing storage and demand flexibility in LV networks," in *Proc. IEEE Manchester PowerTech*, Jun. 2017, pp. 1–6.

[9] H. Li, H. Johra, F. de Andrade Pereira, T. Hong, J. Le Dréau, A. Maturo, M. Wei, Y. Liu, A. Saberi-Derakhtenjani, Z. Nagy, A. Marszal-Pomianowska, D. Finn, S. Miyata, K. Kaspar, K. Nweye, Z. O'Neill, F. Pallonetto, and B. Dong, "Data-driven key performance indicators and datasets for building energy flexibility: A review and perspectives," *Appl. Energy*, vol. 343, Aug. 2023, Art. no. 121217.

[10] A. Dadkhah, B. Vahidi, M. Shafie-khah, and J. P. S. Catalão, "Power system flexibility improvement with a focus on demand response and wind power variability," *IET Renew. Power Gener.*, vol. 14, no. 6, pp. 1095–1103, Apr. 2020.

[11] S. Park and J. Lee, "Dynamic modeling of flexible loads for grid applications," *Energy*, vol. 300, Jan. 2023, Art. no. 126832.

[12] M. H. Mohammadi and K. Saleh, "Synthetic benchmarks for power systems," *IEEE Access*, vol. 9, pp. 162706–162730, 2021.

[13] A. Gupta and P. Singh, "Optimal control strategies for der integration in distribution systems," *Renew. Energy*, vol. 205, pp. 87–99, Jun. 2023.

[14] T. Nguyen and D. Tran, "Strategic placement of pv and battery systems for enhanced grid stability," *Energy Convers. Manage.*, vol. 284, Aug. 2023, Art. no. 117056.

[15] V. Sharma and R. Patel, "Flexible demand management in distribution systems: A review," *Energy*, vol. 251, Oct. 2022, Art. no. 123456.

[16] M. Alam and S. Rahman, "Pv integration in distribution networks: Challenges and solutions," *J. Renew. Sustain. Energy*, vol. 13, Jul. 2021, Art. no. 063101.

[17] M. Trabelsi, M. Massaoudi, I. Chihi, L. Sidhom, S. S. Refaat, T. Huang, and F. S. Oueslati, "An effective hybrid symbolic regression–deep multilayer perceptron technique for PV power forecasting," *Energies*, vol. 15, no. 23, p. 9008, Nov. 2022.

[18] T. Wu, X. Ji, G. Wang, Y. Liu, Q. Yang, Z. Bao, and J. Peng, "Hydrogen energy storage system for demand forecast error mitigation and voltage stabilization in a fast-charging station," *IEEE Trans. Ind. Appl.*, vol. 58, no. 2, pp. 2718–2727, Mar. 2022.

[19] R. Manojkumar, C. Kumar, and S. Ganguly, "Optimal demand response in a residential PV storage system using energy pricing limits," *IEEE Trans. Ind. Informat.*, vol. 18, no. 4, pp. 2497–2507, Apr. 2022.

[20] H. A. Taha, M. H. Alham, and H. K. M. Youssef, "Multi-objective optimization for optimal allocation and coordination of wind and solar DGs, BESSs and capacitors in presence of demand response," *IEEE Access*, vol. 10, pp. 16225–16241, 2022.

[21] V. Vijayan, A. Mohapatra, and S. N. Singh, "Demand response with volt/var optimization for unbalanced active distribution systems," *Appl. Energy*, vol. 300, Oct. 2021, Art. no. 117361.

[22] M. Yao, D. K. Molzahn, and J. L. Mathieu, "An optimal power-flow approach to improve power system voltage stability using demand response," *IEEE Trans. Control Netw. Syst.*, vol. 6, no. 3, pp. 1015–1025, Sep. 2019.

[23] T. Kerdphol, Y. Qudaih, and Y. Mitani, "Optimum battery energy storage system using PSO considering dynamic demand response for microgrids," *Int. J. Electr. Power Energy Syst.*, vol. 83, pp. 58–66, Dec. 2016.

[24] N. Nacar Cikan and M. Cikan, "Reconfiguration of 123-bus unbalanced power distribution network analysis by considering minimization of current & voltage unbalanced indexes and power loss," *Int. J. Electr. Power Energy Syst.*, vol. 157, Jun. 2024, Art. no. 109796.

[25] D. M. Reddy, D. Dwivedi, P. K. Yemula, and M. Pal, "Causal network analysis to study evolution of distribution system with DER integration," *IET Conf. Proc.*, vol. 2023, no. 6, pp. 236–240, Jul. 2023.

[26] J. Jian, J. Zhao, H. Ji, L. Bai, J. Xu, P. Li, J. Wu, and C. Wang, "Supply restoration of data centers in flexible distribution networks with spatial–temporal regulation," *IEEE Trans. Smart Grid*, vol. 15, no. 1, pp. 340–354, Jan. 2023.

[27] S. Xia, S. Bu, C. Wan, X. Lu, K. W. Chan, and B. Zhou, "A fully distributed hierarchical control framework for coordinated operation of DERs in active distribution power networks," *IEEE Trans. Power Syst.*, vol. 34, no. 6, pp. 5184–5197, Nov. 2019.

[28] Y. Liu, J. Li, and L. Wu, "Coordinated optimal network reconfiguration and voltage regulator/DER control for unbalanced distribution systems," *IEEE Trans. Smart Grid*, vol. 10, no. 3, pp. 2912–2922, May 2019.

[29] X. Lu, S. Xia, G. Sun, J. Hu, W. Zou, Q. Zhou, M. Shahidehpour, and K. W. Chan, "Hierarchical distributed control approach for multiple on-site DERs coordinated operation in microgrid," *Int. J. Electr. Power Energy Syst.*, vol. 129, Jul. 2021, Art. no. 106864.

[30] W. Liu and F. Ding, "Hierarchical distribution system adaptive restoration with diverse distributed energy resources," *IEEE Trans. Sustain. Energy*, vol. 12, no. 2, pp. 1347–1359, Apr. 2021.

[31] A. R. Malekpour, A. M. Annaswamy, and J. Shah, "Hierarchical hybrid architecture for volt/var control of power distribution grids," *IEEE Trans. Power Syst.*, vol. 35, no. 2, pp. 854–863, Mar. 2020.

[32] Y. Weng, Q. Lei, R. Ayyanar, V. Vittal, and B. Yang, "Enhancing grid reliability and resilience through novel der control, total situational awareness, and integrated distribution-transmission representation," OSTI, Oak Ridge, Tennessee, Tech. Rep. DOE-ASU-00087731, 2024.

[33] A. Zarei and N. Ghaffarzadeh, "Optimal demand response-based ac opf over smart grid platform considering solar and wind power plants and esss with short-term load forecasts using lstm," *J. Sol. Energy Res.*, vol. 8, no. 2, pp. 1367–1379, 2023.

[34] J. A. Azzolini, M. J. Reno, N. S. Gurule, and K. A. W. Horowitz, "Evaluating distributed PV curtailment using quasi-static time-series simulations," *IEEE Open Access J. Power Energy*, vol. 8, pp. 365–376, 2021.

[35] K. Prabakar, Y. N. Velaga, R. Meadows, B. McGilton, T. Greco, J. Salmon, K. Hill, and L. Tinney, "Understanding line losses and transformer losses in rural isolated distribution systems," Nat. Renew. Energy Lab. (NREL), Golden, CO, USA, Tech. Rep. NREL/CP-5D00-88937, 2024.
[36] D. Pudjianto, P. Djapic, G. Strbac, E. T. van Schalkwyk, and B. Stojkovska, "DER reactive services and distribution network losses," in *Proc. CIRED Berlin Workshop (CIRED)*, vol. 2020, Sep. 2020, pp. 541–544.
[37] X. Wu, C. Yang, G. Han, Z. Ye, and Y. Hu, "Energy loss reduction for distribution networks with energy storage systems via loss sensitive factor method," *Energies*, vol. 15, no. 15, p. 5453, Jul. 2022.
[38] R. F. Arritt and R. C. Dugan, "The IEEE 8500-node test feeder," in *Proc. IEEE PES T&D*, Apr. 2010, pp. 1–6.

MOHAMED MASSAOUDI (Member, IEEE) received the M.Eng. degree in energy engineering from the National Engineering School of Monastir (ENIM), University of Monastir, Tunisia, in 2018, the Ph.D. degree in electronics engineering from the National Institute of Applied Sciences and Technology (INSAT), University of Carthage, Tunisia, in 2021, and the second Ph.D. degree in electrical and computer engineering from Texas A&M University (TAMU), College Station, TX, USA, in 2024.

He has eight years of hands-on experience in applying deep learning and machine learning strategies to tackle real-world problems. During his work at Texas A&M University at Qatar, he is the lead author of more than 50 peer-reviewed journal and conference publications and three book chapters. His research interests include AI applications for demand flexibility, cybersecurity in smart grids, and innovative prediction models. He was a recipient of the Outstanding Student Research Excellence Award, in 2021; the Thomas W. Powell'62 and Powell Industries Inc., Fellowship Award, in 2024; the Best Paper Presentation Recognition in the IECON24; and the Richard E. Ewing Award for Excellence, in 2024, for his research contributions. His H-index is 16 and his work has been cited more than 1200 times.

KATHERINE R. DAVIS (Senior Member, IEEE) received the B.S. degree in electrical engineering from The University of Texas at Austin, Austin, TX, USA, in 2007, and the M.S. and Ph.D. degrees in electrical engineering from the University of Illinois at Urbana–Champaign, Champaign, IL, USA, in 2009 and 2011, respectively. She is currently an Associate Professor of electrical and computer engineering with Texas A&M University, College Station, TX, USA. Her research interests include the operation and control of power systems, interactions between computer networks and power networks, security-oriented cyber-physical analysis techniques, and data-driven and model-based coupled infrastructure analysis and simulation.

KHANDAKER AKRAMUL HAQUE (Graduate Student Member, IEEE) received the B.S. and M.S. degrees in electrical and electronic engineering from Bangladesh University of Engineering and Technology, Dhaka, Bangladesh, in 2015 and 2020 respectively. He is currently pursuing the Ph.D. degree in electrical and computer engineering with Texas A&M University, TX, USA. His research interests include grid resilience, cybersecurity, machine learning, and modeling and containerization of large cyber-physical systems.